Piezotronic Effect Modulated Heterojuction Electron Gas in AlGaN/AlN/GaN Heterostructure Microwire

Xingfu Wang, Ruomeng Yu, Chunyan Jiang, Weiguo Hu, Wenzhuo Wu, Yong Ding, Wenbo Peng, Shuti Li, and Zhong Lin Wang**

1D semiconductor nanowires (NWs) have attracted considerable attentions for various applications such as light-emitting diode,[1,2] laser,[3,4] field-effect transistor,[5,6] and nanogenerator[7–10] due to their unique structures and enhanced mobility caused by the 1D quantum confinement effects to outperform their planar counterparts. However, the carrier mobility degradation, resulted from scatterings of charged dopant centers, has long been an inevitable obstacle to the performances of devices fabricated with doped NWs for practical applications. To overcome this issue, low-dimensional carrier (electron or hole) gases observed in semiconductor heterostructure NWs, such as Ge/Si,[11] AlGaAs/GaAs,[12] and AlGaN/GaN,[13] have been extensively studied. By utilizing ionic charges from spontaneous polarization and lattice mismatch at local heterojunctions, the carrier transport channel is spatially separated from the ionized impurities via band structure engineering, and thus the impurity scattering is significantly reduced/eliminated with the carrier mobility substantially enhanced. Among several III-nitride heterostructures, AlGaN/GaN is one of the most promising material systems for creating heterojunction electron gas (HEG) due to its strong intrinsic polarizations,[14] and has been widely applied for high electron mobility transistor (HEMT)[13] and other high-performance quantum electronics.[15] In previous reports, tuning alloy compositions and controlling the thickness of AlGaN layer are two most effective ways to tune/control the physical properties of HEG and thus essential to optimizing devices performances.[16,17] However, the extreme complexity and high expenses of these two methods are preventing them from practical applications. Therefore, it is necessary to develop new approaches for easier and more effective modulations of HEG in HEMTs as alternatives.

X. Wang, R. Yu, Dr. W. Wu, Dr. Y. Ding, W. Peng, Prof. Z. L. Wang
School of Materials Science and Engineering
Georgia Institute of Technology
Atlanta, GA 30332-0245, USA
E-mail: zhong.wang@mse.gatech.edu
X. Wang, Prof. S. Li
Guangdong Provincial Key Laboratory of Nanophotonic Functional Materials and Devices
Guangdong Engineering Technology Research Center of Optoelectronic Functional Materials and Devices
Institute of Optoelectronic Materials and Technology
South China Normal University
Guangzhou 510631, China
E-mail: lishuti@scnu.edu.cn
C. Jiang, Prof. W. Hu, Prof. Z. L. Wang
Beijing Institute of Nanoenergy and Nanosystems
Chinese Academy of Sciences
Beijing 100083, China

DOI: 10.1002/adma.201601721

The piezotronic effect is a two-way coupling effect between piezoelectric and semiconductor properties found in semiconductor materials with noncentrosymmetric crystal structures. By utilizing strain-induced piezoelectric polarization charges presented at local interface/junction to modify the energy band structures, the piezotronic effect has been applied to tune/control the electric transport properties of NWs transistors,[18] bio/chemical sensors,[19–21] and logic circuits.[22] As wurtzite structured III-nitride semiconductors, AlGaN/GaN heterostructure possesses both piezoelectric and semiconductor properties. Upon straining, piezoelectric polarization charges created by mechanical deformations combine with the intrinsic spontaneous and lattice-mismatch-induced polarizations at local heterojunction and effectively modify the energy profile. The corresponding physical properties of HEG as well as the electric transport properties of AlGaN/GaN heterostructure based HEMTs are therefore modified by the piezotronic effect. This approach is fundamentally new in science and simple to apply without adding extra costs to the device fabricating processes.

In this work, lateral AlGaN/AlN/GaN heterostructured microwires orientated along *a*-axis are synthesized by metal organic chemical vapor deposition (MOCVD). The existence of HEG in AlGaN/AlN/GaN microwires is proved by both experimental and simulation results. The piezotronic effect is then introduced to modulate the physical properties of electron gas near heterojunctions at various temperatures ranging from 77 to 300 K. Theoretical simulations are conducted via the finite element analysis (FEA) and self-consistent numerical calculation to systematically illustrate and confirm the proposed working mechanism. This study provides in-depth understandings about the piezotronic-effect modulation of low-dimensional electron gas in heterostructured nanomaterials and indicates potential applications in HEMTs and MEMS/NEMS.

AlGaN/AlN/GaN heterostructure microwires used in this work are synthesized on patterned Si substrate by MOCVD as shown in **Figure 1**a. Detailed synthesizing processes are found in the Experimental Section. Undoped single-compound GaN microwires with uniform lateral facets are grown first and serve as a platform to sequentially deposit undoped AlN and AlGaN layers. The cross-section high-angle annular dark-field scanning transmission electron microscopy (HAADF-STEM) image of an individual AlGaN/AlN/GaN heterostructure microwire is presented in Figure 1b, showing a trapezoidal

© 2016 WILEY-VCH Verlag GmbH & Co. KGaA, Weinheim

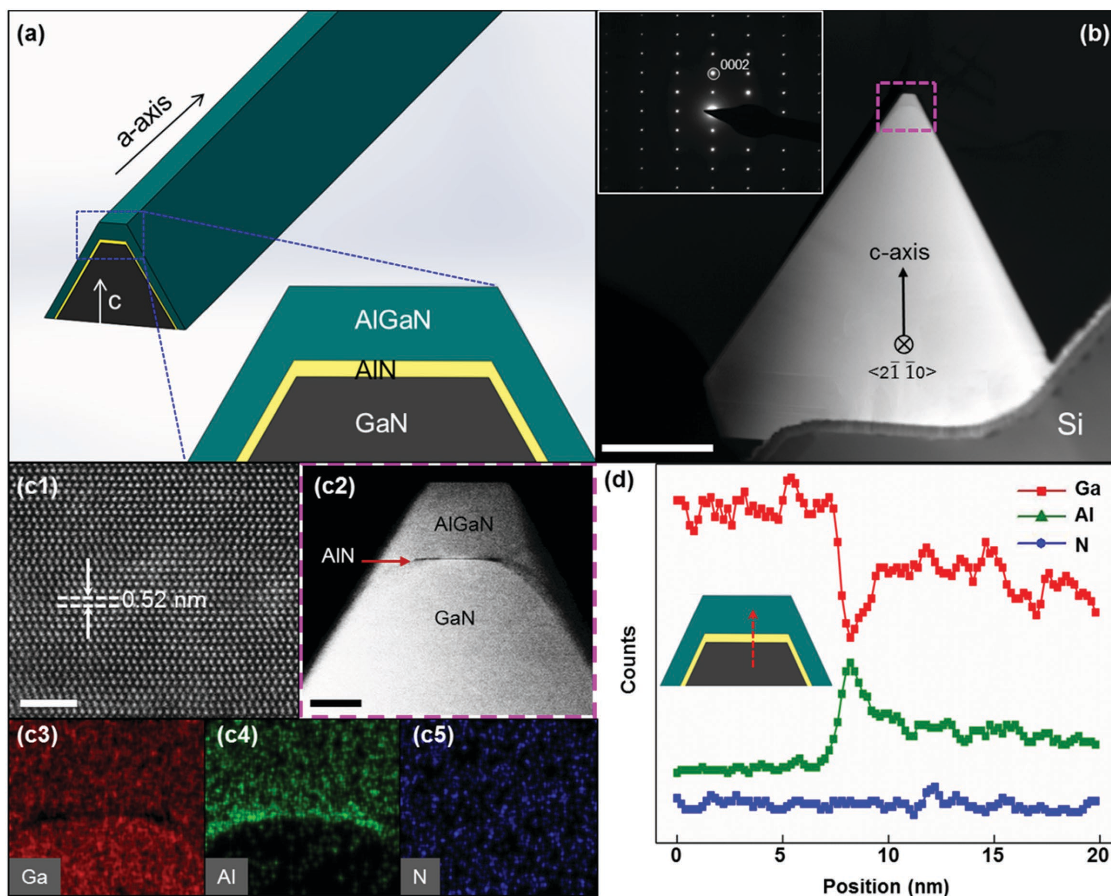

Figure 1. Structure characterizations of AlGaN/AlN/GaN heterostructures microwire. a) Schematic diagram of an individual heterostructure microwire and magnified cross-sectional view of a microwire facet highlighting AlGaN/AlN/GaN structure. b) The cross-section HAADF-STEM image of an individual AlGaN/AlN/GaN heterostructure microwire. The scale bar is 500 nm. Inset: corresponding electron diffraction pattern. c1) High-resolution transmission electron microscope image acquired from GaN. The scale bar is 5 nm. c2) The magnified HAADF-STEM image collected from the labeled area in Figure 1b. The scale bar is 20 nm. c3–5) STEM energy-dispersive X-ray spectroscopy (EDX) elemental mapping of the AlGaN/AlN/GaN heterojunction. d) The EDX line profiles for Ga (red), Al (green), and N (blue) elements.

cross section with top width of ≈100 nm, bottom width of ≈1.5 µm and height of ≈1.5 µm. The corresponding selected area electron diffraction (Tecnai G2) patterns indexed along the *a*-axis (Figure 1b, inset) and the high-resolution transmission electron microscope (FEI F30) image (Figure 1c1) are presented to characterize the crystal structure of AlGaN/AlN/GaN heterostructure microwire as noncentrosymmetric wurtzite single crystal orientated along nonpolar $\langle 2\bar{1}\bar{1}0 \rangle$ (i.e., *a*-axis) direction with polar *c*-axis pointing to its top surface. The magnified HAADF-STEM image collected from the labeled area in Figure 1b is shown in Figure 1c2, clearly presenting a dark contrast line (ultrathin AlN interlayer) sandwiched by the top AlGaN layer and bottom GaN. The thicknesses of AlGaN and AlN layers are estimated to be 40 and 1.6 nm, respectively. STEM energy-dispersive X-ray spectroscopy (EDX) elemental mapping (Figure 1c3–5) of AlGaN/AlN/GaN heterojunction clearly reveals the spatial distributions of Ga, Al, and N elements, confirming that the contrasts in Figure 1c2 are from the variation of chemical compositions. The corresponding line profile extracted from EDX mapping is presented in Figure 1d.

The existence of HEG at AlGaN/AlN/GaN heterojunctions is confirmed by experimental characterizations and theoretical simulations as shown in **Figure 2**. The lattice-resolved HAADF-STEM image shown in Figure 2a indicates that the interfaces of AlGaN/AlN and AlN/GaN are atomically uniform and sharp without obvious boundary defects or dislocations. These results confirm the absence of strain relaxation in AlGaN and AlN epitaxy layers, and suggest that scattering due to surface roughness should be reduced in this heterostructure microwire. The corresponding atomic structure model and conduction band energy profile of the AlGaN/AlN/GaN heterostructure are shown in Figure 2b,c, respectively. Owing to its noncentrosymmetric crystal structure, there are two different types of intrinsic polarizations presented in AlGaN/AlN/GaN heterojunctions: (i) the spontaneous polarization $P^{\mathrm{AlGaN}}_{\mathrm{sp}}$ and $P^{\mathrm{GaN}}_{\mathrm{sp}}$ existing in AlGaN and GaN, respectively; (ii) lattice-mismatch-induced piezoelectric polarizations existing in AlGaN layer (P_{lm}) due to the different lattice constants between AlGaN epitaxy layer and GaN relaxed "substrate."[23] These polarizations lead to the accumulation of net positive fixed charges at AlGaN/AlN/GaN interface. Meanwhile, the conduction band of GaN

© 2016 WILEY-VCH Verlag GmbH & Co. KGaA, Weinheim
Adv. Mater. 2016, DOI: 10.1002/adma.201601721

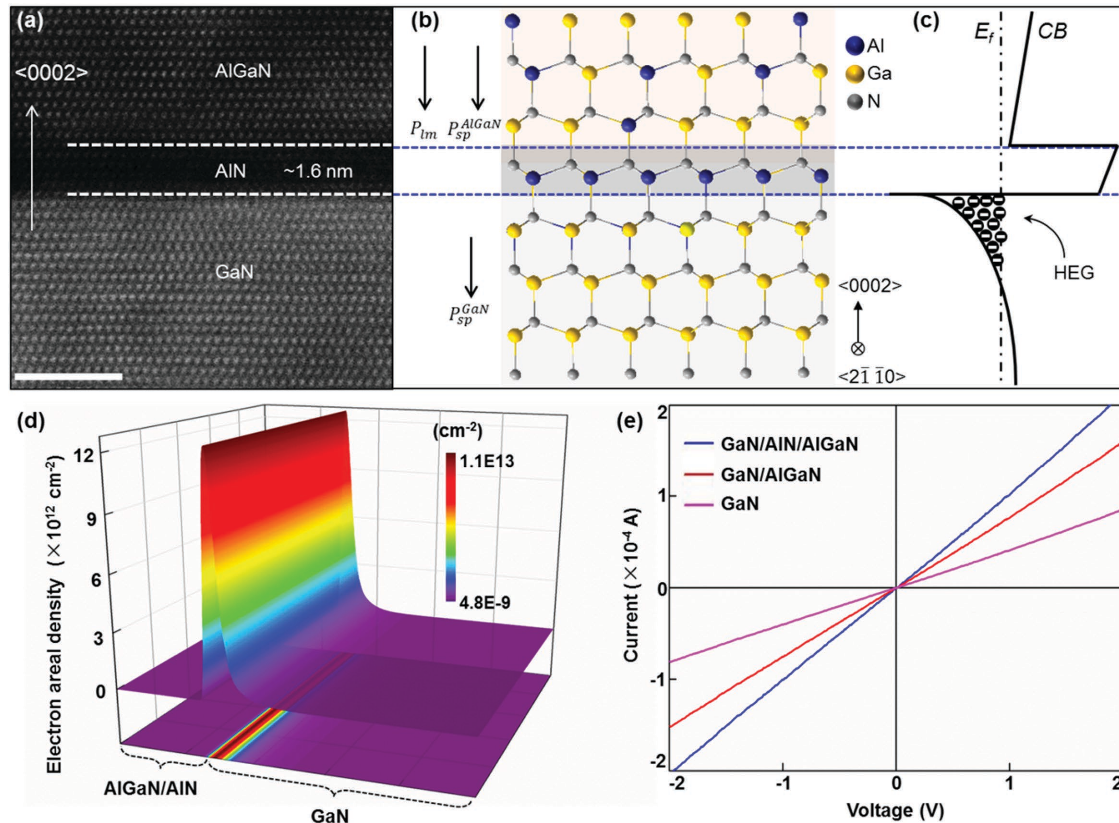

Figure 2. HEG distributed at AlGaN/AlN/GaN heterojunctions. a) The lattice-resolved HAADF-STEM image of the interfacial region of AlGaN/AlN/GaN heterostructure. b) Corresponding atomic structure model. c) Corresponding conduction band profile and the distribution of HEG. d) The calculated electron density distribution in AlGaN/AlN/GaN heterostructure microwire. e) *I–V* characterizations of microwire devices based on AlGaN/AlN/GaN heterostructure microwire, AlGaN/GaN heterostructure microwire and homogeneous single-compound GaN microwire.

lies below that of AlGaN, leading to the formation of a triangle-shaped quantum potential well in GaN layer near the AlN/GaN interface (Figure 2c). As a result, the electrons in heterostructure microwire are attracted and confined in this potential well and HEG is generated. In order to further confirm the existence of HEG, the electron density distribution in the AlGaN/AlN/GaN heterostructure microwire is calculated and shown in Figure 2d, indicating the formation of HEG with a high electron density of 1×10^{13} cm^{-2} locating at a narrow region in GaN layer close to the heterojunction interface. Besides, the ultrathin AlN interlayer is utilized to reduce the alloy scattering from AlGaN layer and provide a large conduction band discontinuity for better confinement of electrons in the potential well.[24]

Enhancements on the electric transport properties of heterostructure microwires by HEG and AlN interlayer are investigated by synthesizing three different microwires: AlGaN/AlN/GaN heterostructure microwire, AlGaN/GaN heterostructure microwire and homogeneous single-compound GaN microwire. Typical *I–V* characteristics of these three types of microwires based two-terminal Ohmic devices are compared in Figure 2e, showing better conductance of AlGaN/GaN microwires than that of GaN due to the existence of HEG, and the best conductance of AlGaN/AlN/GaN microwires because of the reduced electrons scattering from ultrathin AlN interlayer.

The piezotronic effect modulations on the HEG and electric transport properties of AlGaN/AlN/GaN microwire devices are systematically studied under various straining conditions as shown in **Figure 3**. The experimental setups and the schematic of the microwire devices are presented in Figure 3a. Details about fabricating Ohmic devices, applying and calculating strains on devices are illustrated in Experimental Section. *I–V* characteristics of the as-fabricated microwire devices under a series of compressive and tensile strains are measured and summarized in Figure 3b, demonstrating Ohmic transport property. Obviously, the output currents of heterostructure microwire devices increase as increasing compressive strains, and decrease as increasing tensile strains. The conductance of the microwire devices (*G*) and the corresponding relative changes ($\Delta G/G$) are extracted and plotted as a function of applied strains as shown in Figure 3c. It clearly indicates that the conductance of the AlGaN/AlN/GaN heterostructure microwire increases/decreases with the compressive/tensile strain.

The superposition among piezotronic-induced polarization P_{pz}, intrinsic spontaneous polarization $P^{AlGaN}{}_{sp}$ and $P^{GaN}{}_{sp}$, and lattice-mismatch-induced piezoelectric polarization P_{lm} is explored by calculating the fixed polarization charges distributions at the interfaces of AlGaN/AlN/GaN heterostructure. The fixed polarization charges distributed at the bottom surface of

© 2016 WILEY-VCH Verlag GmbH & Co. KGaA, Weinheim

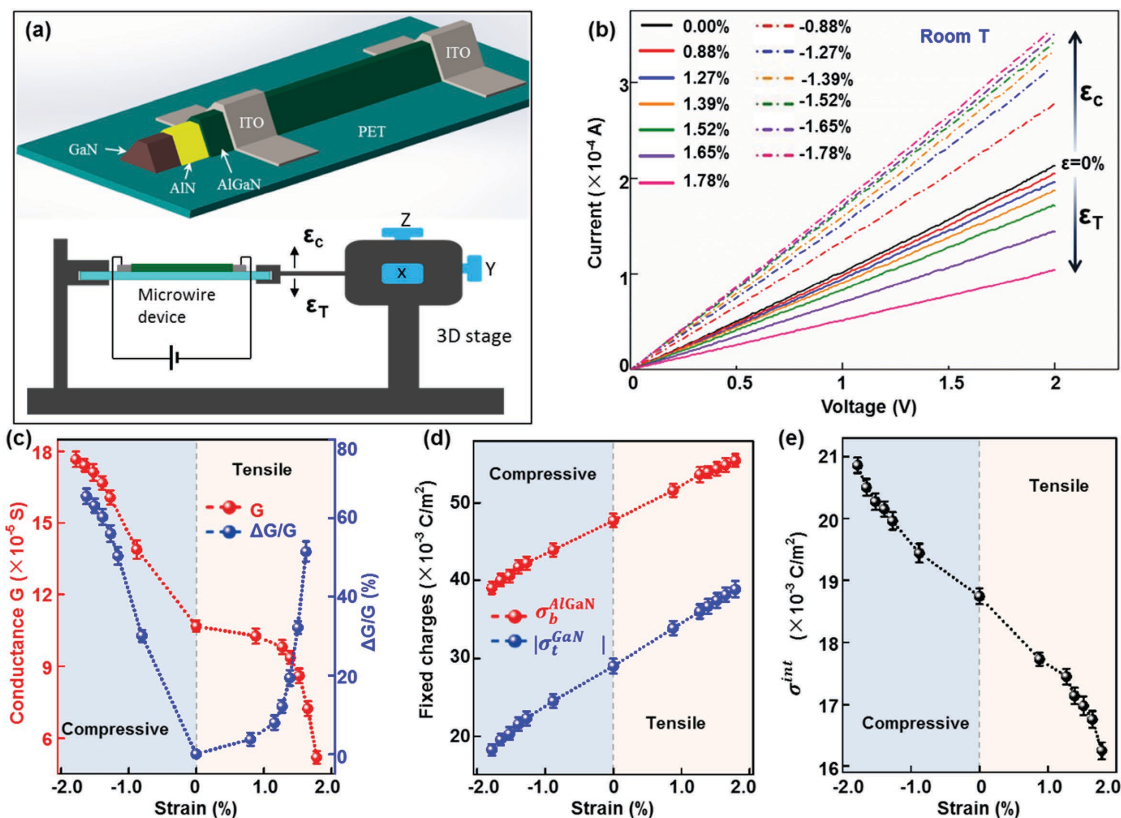

Figure 3. Piezotronic effect and fixed charge distribution in AlGaN/AlN/GaN heterostructure. a) Experimental setups (lower) and the schematics (upper) of the microwire devices. b) *I–V* characteristics of the as-fabricated microwire devices under strain free and a series of compressive and tensile strain condition. c) The conductance (*G*) and the corresponding relative changes (Δ*G*/*G*) of the microwire devices as a function of strains. d) The fixed polarization charges distributed at the bottom surface of AlGaN layer ($\sigma_b^{\mathrm{AlGaN}}$) and the absolute value of fixed polarization charges distributed at the top surface of GaN ($|\sigma_t^{\mathrm{GaN}}|$) as a function of applied external strains. e) The effective net fixed polarization charges (σ^{int}) at AlGaN/AlN/GaN heterojunctions as a function of externally applied strains.

AlGaN layer ($\sigma_b^{\mathrm{AlGaN}}$) and the absolute value of fixed polarization charges distributed at the top surface of GaN ($|\sigma_t^{\mathrm{GaN}}|$) as a function of externally applied strains are first calculated and summarized in Figure 3d. Then, the effective net fixed polarization charges (σ^{int}) at the AlGaN/AlN/GaN heterojunction as a function of externally applied strains are also calculated and shown in Figure 3e. Detailed calculation process is found in the Supporting Information (Supplementary Methods). It is clear that σ^{int} is always positive with or without external strains with the value increasing/decreasing as compressive/tensile strains. Therefore, more effective polarization charges accumulate at the heterojunctions as increasing compressive strains, while less effective polarizations present as applying more tensile strains to the devices. These changes agree well with the observed *I–V* curves in Figure 3b and are resulted from the modulations of energy band profiles at heterojunctions by the piezotronic effect.

Temperature dependence of the piezotronic effect modulations of HEG at AlGaN/AlN/GaN heterojunctions is systematically investigated as shown in **Figure 4**. The schematic and digital images of the micromanipulation cryogenic probe system (Janis, model ST-500-2) used are shown in Figure S1a,b (Supporting Information), respectively. Details about the fabrication of microwire devices, configuration of the low temperature system and the measurement method have been illustrated in our previous reports.[25,26] *I–V* characteristics of AlGaN/AlN/GaN heterostructure microwire devices are measured at 300 (Figure 4a), 230 (Figure S1c, Supporting Information), 170 (Figure 4b), 110 (Figure S1d, Supporting information), and 77 K (Figure 4c) by externally applying compressive and tensile strains along *a*-axis. Obviously, the output currents increase as applying compressive strains and decreases as applying tensile strains at each temperature condition but with distinguishable magnitudes. As the system temperature decreases, the changes of *I–V* curves become more and more significant, and the difference among output currents derived under various straining conditions become most explicit at 77 K. These results are resulted from the enhanced piezotronic effect at low temperature as freeze-out effect reduces the screening again piezo-polarizations at lower temperature,[24] and thus the enhanced piezotronic effect at lower temperature condition plays a more significant role in modifying the energy profiles and physical properties of HEG at AlGaN/AlN/GaN heterojunctions.

Conductances (*G*) of the AlGaN/AlN/GaN heterostructure microwire devices at each temperature as a function of external strains are plotted in Figure 4d. Obviously, the conductance of the microwire devices at each straining condition increases with the temperature since higher carrier mobility obtained at

© 2016 WILEY-VCH Verlag GmbH & Co. KGaA, Weinheim
Adv. Mater. 2016, DOI: 10.1002/adma.201601721

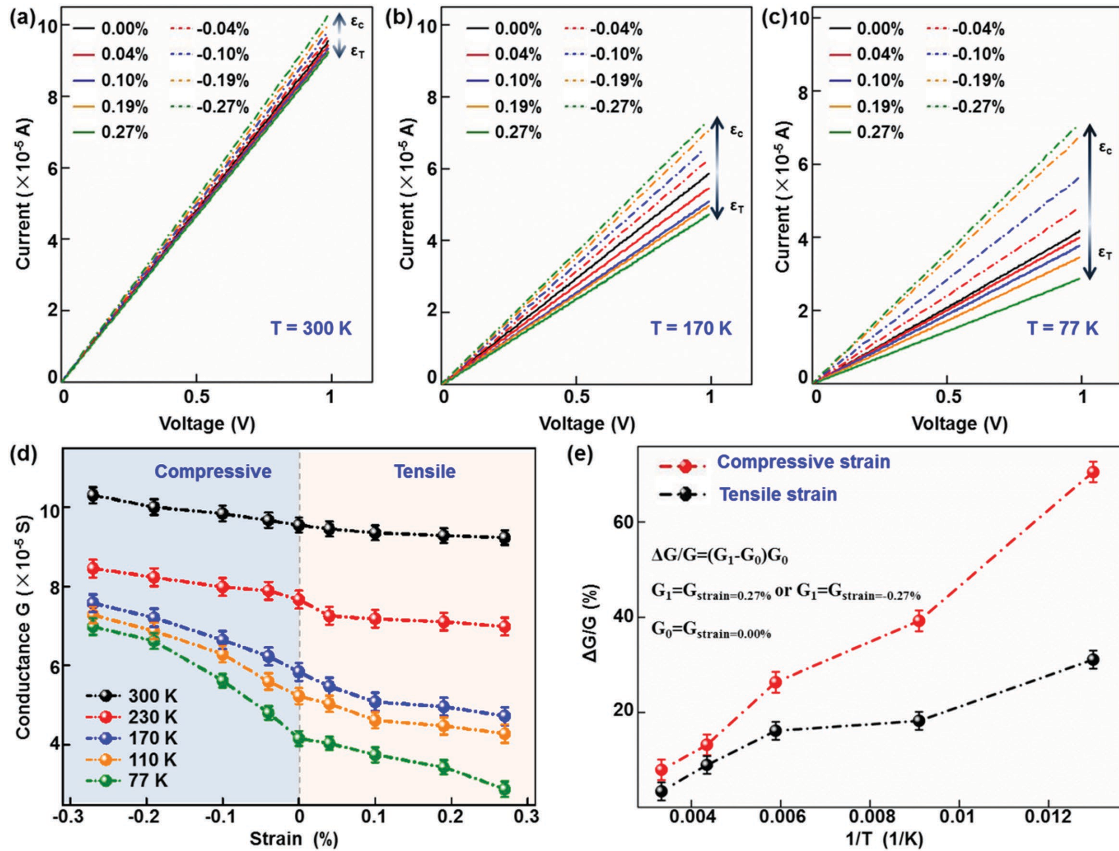

Figure 4. Temperature dependence of the modulation of HEG by the piezotronic effect. *I–V* characteristics of AlGaN/AlN/GaN heterostructure microwire devices at a) 300 K, b) 170 K, and c) 77 K under externally applied compressive and tensile strains along *a*-axis. d) Conductances (*G*) of AlGaN/AlN/GaN heterostructure microwire devices under each temperature condition as a function of external strains. e) The relative changes of conductance under compressive (red) and tensile (black) strain conditions.

higher temperature due to more thermal energies. Moreover, at each temperature condition, the conductance of heterostructure microwire devices shows a consistent increasing and decreasing tendency as the increasing of compressive and tensile strain, respectively. This variation tendency becomes more and more significant as changing the temperature from 300 to 77 K. Further study of the temperature dependence of piezotronic effect modulation of HEG at heterojunctions is conducted by calculating the relative changes of conductance $\Delta G/G = (G_1 - G_0)G_0$, where $G_0 = G_{\text{strain} = 0.00\%}$; $G_1 = G_{\text{strain} = -0.27\%}$ or $G_1 = G_{\text{strain} = 0.27\%}$ as shown in Figure 4e. For compressive strains, the calculated $\Delta G/G$ increases by 890% as changing the ambient temperature from 300 to 77 K; for tensile strains, the calculated $\Delta G/G$ increases by 940% from 300 to 77 K. These results indicate that the modulations of HEG and electric transport properties of AlGaN/AlN/GaN heterostructure microwires become substantially more effective at lower temperature due to the enhanced piezotronic effect.

Energy diagrams of the AlGaN/AlN/GaN heterostructure microwire along *c*-axis are carefully analyzed under different straining conditions to illustrate the working mechanism of piezotronic effect modulations of HEG at heterojunctions. Under strain free condition (**Figure 5**a), a triangle-shape potential well is formed in GaN close to AlN/GaN interface due to the co-existence of $P^{\text{AlGaN}}{}_{\text{sp}}$, P_{lm}, and $P^{\text{AlGaN}}{}_{\text{sp}}$ and the large band discontinuity between AlGaN and GaN. The net fixed charges at AlGaN/AlN/GaN heterojunctions σ^{int} are always positive with or without strains (Figure 3e). Therefore, free electrons within the microwire close to the heterostructure interface are attracted by σ^{int} and confined in the potential well, giving rise to the formation of HEG as shown in Figure 5a. Under compressive strain along *a*-axis of the microwire (i.e., tensile strain along *c*-axis), positive piezoelectric polarization charges (piezo-charges) are induced at +*c* plane while negative piezo-charges at −*c* plane. The energy band of AlGaN close to AlGaN/AlN interface tilts upward by the negative piezo-charges and the energy band of GaN near GaN/AlN interface is bent downward by positive piezo-charges as shown in Figure 5b. Thus the potential well becomes "deeper" to confine more electrons in it due to the modulations of energy profile at heterojunctions. Meanwhile, the increased σ^{int} under compressive strain attracts more free electrons, thus the sheet density of HEG increases. This agrees well with the enhanced electric transport of heterostructure microwire shown in Figure 3b. In contrast, under tensile strain along *a*-axis (Figure 5c), energy band of AlGaN close to AlGaN/AlN interface is bent downward by the positive piezo-charges and the energy band of GaN near GaN/AlN interface is elevated by negative piezo-charges. Thus, the potential well becomes "shallower" compared to strain free condition and the corresponding electrons confinement is weakened. Meanwhile,

© 2016 WILEY-VCH Verlag GmbH & Co. KGaA, Weinheim

ADVANCED MATERIALS
www.advmat.de

Materials Views
www.MaterialsViews.com

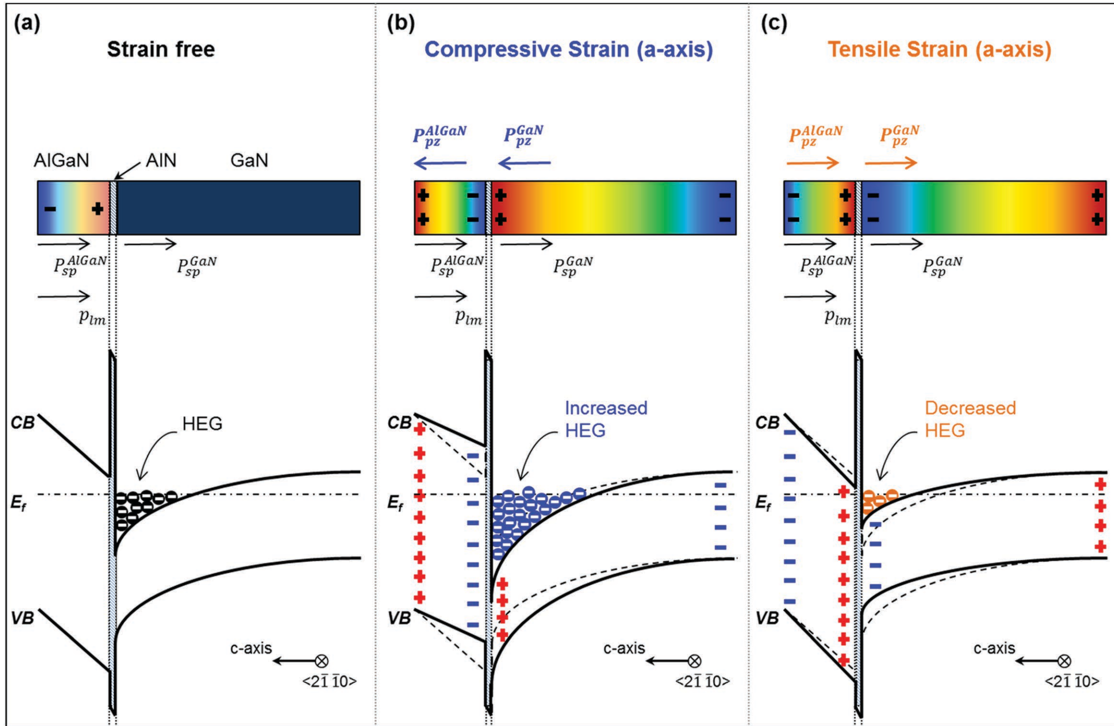

Figure 5. Working mechanism of the piezotronic effect modulations of HEG. The coupling of spontaneous polarization, lattice-mismatch-induced polarization, piezotronic-effect-induced polarization, corresponding energy band profiles, and the distribution of HEG in AlGaN/AlN/GaN heterostructures microwire under (a) strain free, (b) compressive strain along *a*-axis, and (c) tensile strain along *a*-axis conditions.

the decreased σ^{int} under tensile strain releases a certain amount of the confined free electrons from the potential well and thus decreases the sheet density of HEG. This leads to the reduced electric transport of heterostructure microwire, which is consistent with the experimental result shown in Figure 3b.

To confirm the proposed physical mechanism, modulations of HEG by the piezotronic effect in AlGaN/AlN/GaN heterostructure microwire is further studied by self-consistent numerical calculations. Under the effective mass approximation, the electronic sub-band states in the growth direction of the AlGaN/AlN/GaN heterojunction are solutions to the Schrödinger wave equation[27,28]

$$-\frac{h^2}{2}\frac{\mathrm{d}}{\mathrm{d}z}\left[\frac{1}{m^*}\frac{\mathrm{d}\Psi_i(z)}{\mathrm{d}z}\right]+\left[V(z)-E_i\right]\Psi_i(z)=0 \tag{1}$$

where m^* is referring to the electron effective mass at the conduction-band edge, $V(z)$ is potential energy, E_i indicates the energy of the ith sub-band, and $\Psi_i(z)$ denotes the wave function. The nonparabolicity of the conduction band can be ignored, m^* is independent of electron energy. Here, $m^* = 0.22\ m_0$ and $m^* = 0.242\ m_0$ for GaN and $Al_{0.3}Ga_{0.7}N$, respectively. The potential energy $V(z)$ can be expressed as

$$V(z)=V_c(z)+V_h(z)+V_{xc}(z) \tag{2}$$

in which $V_c(z)$ is the conduction-band edge potential in a form of the step-function associated with the conduction band offset at the AlGaN/AlN/GaN heterojunction, $V_h(z)$ is the Hartree potential of the electrostatic interaction due to mobile and immobile charges distributed in the system, and $V_{xc}(z)$ is the exchange-correlation potential representing the many-body interactions and is not included in the $V_h(z)$. $V_h(z)$ is the solution to the Poisson's equation

$$\frac{\mathrm{d}}{\mathrm{d}z}\left[k(z)\frac{\mathrm{d}}{\mathrm{d}z}V_h(z)\right]=e^2\varphi(z) \tag{3}$$

in which k is the dielectric constant which is assumed to be changed abruptly at the AlGaN/AlN/GaN heterojunction. The density of total charges $\varphi(z)$ is given as

$$\varphi(z)=\sum_{j=t,i,b}\sigma(z)\delta(z-z_i)+p(z)+N_D^+(z)-n(z)-N_A^-(z) \tag{4}$$

where $\sigma(z)$, $p(z)$, $N_D^+(z)$, $n(z)$, and N_A^- represent the density of immobile polarization charges, the density of free holes induced in the p-channel, the density of ionized donors, the density of free electrons in the n-channel, and the density of ionized acceptors, respectively. $\sigma(z)$ contains the immobile polarization charges distributed at the boundary or the interface of AlGaN/AlN/GaN heterostructure, which is sensitive to the external applied strains and can be obtained by FEA calculation (Supplementary Methods, Supporting Information). $p(z)=N_A^-(z)=0$ is adopted to the n-type AlGaN and GaN in this work. From the neutrality condition, the following conditions must be satisfied for the sum of total charges

© 2016 WILEY-VCH Verlag GmbH & Co. KGaA, Weinheim

$$\int_{z_t}^{z_b} \rho(z)\,\mathrm{d}(z) = 0 \tag{5}$$

Considering AlGaN/AlN/GaN heterostructure microwire used in this work with HEG channel formed at the heterojunction, $n(z)$ is given as

$$n(z) = \sum_i n_{s_i} \left|\Psi_i(z)\right|^2 \tag{6}$$

in which n_{s_i} is the sheet charge density of electrons in the ith sub-band which is represented below as a function of effective mass

$$n_{s_i} = \frac{m^* k_B T}{\pi\hbar^2} \ln\left[1 + \exp\left(\frac{E_F - E_i}{K_B T}\right)\right] \tag{7}$$

Here, k_B and T are the Boltzmann constant and the electron temperature, respectively. The Fermi energy, (E_F), is determined from the condition that the sum of sub-band electron densities is equal to the total electron density N_e

$$N_e = \int_{z_t}^{z_b} n(z)\,\mathrm{d}(z) = \sum_i n_i \tag{8}$$

N_e can be determined in a self-consistent manner using two boundary conditions for Fermi-level pinning at the upper and the lower boundaries of the system.

The density of positively ionized donors $N_D^+(z)$ in Equation (4) can be written as

$$N_D^+(z) = N_D(z) f_D^+(z) \tag{9}$$

where $N_D(z)$ is the concentration of donor impurities distributed in the system, and $f_D^+(z)$ is the probability that a donor state with a degeneracy factor of 2 at energy $E_D(z)$ is ionized by losing an electron

$$f_D^+(z) = 1 - \frac{1}{1 + \frac{1}{2}\exp\left[\frac{E_D(z) - E_F}{K_B T}\right]} \tag{10}$$

in this work, $E_D(z)$ is assumed to be 0.2 eV below the conduction band of $Al_{0.3}Ga_{0.7}N$.

$V_{xc}(z)$ in Equation (2) can be formulated using a density functional theory. In the simplest approximation, the so-called local density approximation, $V_{xc}(z)$ can be parameterized in an analytic form

$$V_{xc}(z) = -\left[1 + \frac{0.7734 r_s}{21} \ln\left(1 + \frac{21}{r_s}\right)\right] \frac{2E_R}{\pi\alpha r_s} \tag{11}$$

where $\alpha = \left(\frac{4}{9\pi}\right)^{1/3}$, and r_s is the radius of a sphere containing one electron

$$r_s = \left[\frac{4}{3}\pi a^{*3} n(z)\right]^{-1/3} \tag{12}$$

In the unit of the effective Bohr radius, the effective Rydberg energy is given by

$$E_R = \frac{e^2}{8\pi k a^*} \tag{13}$$

$V_{xc}(z)$ gives a significant effect on the electronic sub-band states and the bandgap with an increase of electron density.

The electron wave function $\Psi_i(z)$ at the top surface of AlGaN layer and the bottom surface of GaN is set to be zero, which is defined as the boundary conditions. Furthermore, the potential energy at the top surface of AlGaN is defined as 1.46 eV, which is assumed as the initial value for the calculation. Schrödinger wave equation and the Poisson's equation are calculated iteratively until self-consistency is achieved.

The calculated conduction band of the AlGaN/AlN/GaN heterostructure and corresponding sheet density of HEG under strain free condition are shown in Figure S2a (Supporting Information), indicating that an obvious potential well is induced in GaN close to AlN/GaN interface and the HEG with high sheet density up to 1.1×10^{13} cm^{-2} is formed and distributed within the potential well. The conduction band energy profiles (E_c) under compressive strains along a-axis of the heterostructure microwire are derived and plotted in **Figure 6**a. The calculated E_c at AlGaN/AlN heterojunction (labeled by a red rectangular box) and that at AlN/GaN heterojunction (labeled by a blue rectangular box) are enlarged and shown in Figure 6b,c, respectively. It is clear that, as increasing compressive strains, E_c of AlGaN close to the AlGaN/AlN heterojunction tilts upward and E_c of GaN near the AlN/GaN heterojunction lowers down. The corresponding calculation results of E_c under various tensile strains are shown in Figure S1b–d, indicating the contrary that as increasing tensile strains, E_c of AlGaN close to the AlGaN/AlN heterojunction is bent downward and E_c of GaN near the AlN/GaN heterojunction moves upward. The sheet density of HEG confined in the potential well under strain free, compressive and tensile straining conditions are plotted in Figure 6d. The corresponding peak values of HEG sheet density are extracted and plotted in Figure 6e, clearly showing that the HEG density increases with the compressive strain and decreases with the tensile strain. These calculated results above completely agree with and further confirm the proposed physical mechanism in Figure 5.

The piezotronic effect is applied to AlGaN/AlN/GaN heterostructure microwires as a novel approach to modulate the physical properties of HEG and thus tune/control the electric transport process of carriers across heterojunctions. Unlike previously reported methods by either modifying the alloy components or controlling the thickness of each layer to modulate the HEG properties, here we utilize strain-induced piezoelectric polarization charges to modify the energy band profile at local heterojunctions as an effective way for physical properties modulations of HEG. Compared with traditional methods, this approach is fundamentally new in science and possesses huge advantages, such as easy-to-fabricate, low costs as well as being modulated post sample growth by applying an external strain. By introducing the piezotronic effect to AlGaN/AlN/GaN heterostructure microwires, at room temperature, the

© 2016 WILEY-VCH Verlag GmbH & Co. KGaA, Weinheim

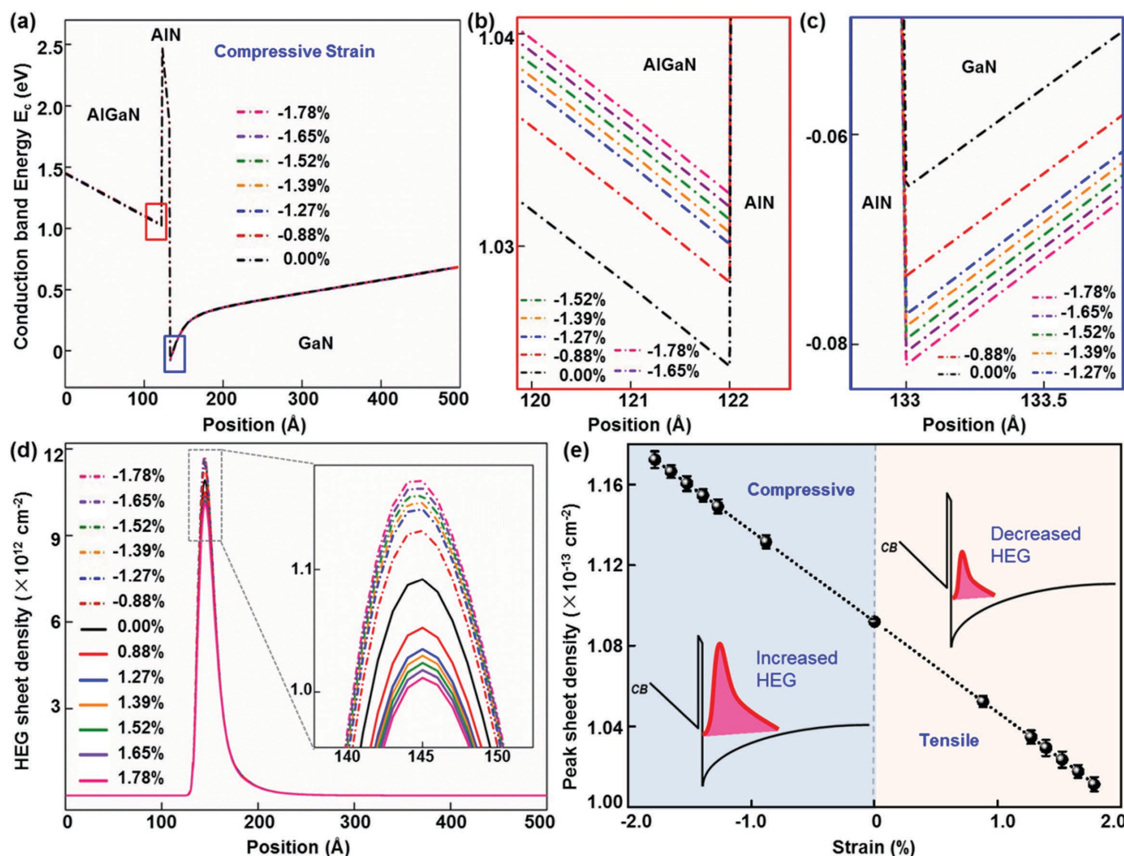

Figure 6. Self-consistent calculation of energy profiles and HEG sheet density. a) The conduction band energy profiles under strain free and compressive strains along *a*-axis of the heterostructure microwire. b) The enlarged E_c at AlGaN/AlN heterojunction as labeled by red rectangular box in (a). c) The enlarged E_c at AlN/GaN heterojunction as labeled by blue rectangular box in (a). d) The sheet density of HEG confined in the potential well under strain free, compressive, and tensile strain conditions. e) Corresponding peak values of HEG sheet density extracted from (d).

conductance is increased by 165% under –1.78% compressive strains, and reduced by 48% under 1.78% tensile strains; at 77 K, this modulating effect is further improved by 890% and 940% under compressive and tensile strains, respectively, due to the enhanced piezotronic effect at low ambient temperature. Theoretical simulations are conducted via FEA and self-consistent numerical calculation to systematically illustrate and confirm the proposed working mechanism. The calculated interface polarization charges, energy profile and electron sheet density distribution under various straining conditions demonstrate that the sheet density of HEG increases with compressive strains and decreases with tensile strains. This study provides in-depth understanding about the piezotronic-effect modulation of low-dimensional electron gas in heterostructured nanomaterials, with potential applications in HEMTs and MEMS/NEMS.

Experimental Section

Synthesizing AlGaN/AlN/GaN Heterostructure Microwires: First, a 100 nm thick SiO_2 film was deposited on Si (100) substrates by plasma-enhanced chemical vapor deposition. Second, periodic stripes (5 μm spacing, 5 μm width) of SiO_2 along the $\langle 11\bar{2}0\rangle$ direction were formed by photolithography and wet chemical etching. Third, 1 μm deep trapezoidal grooves with two opposed Si (111) facets separated by a bottom Si (100) facet were fabricated through anisotropic etching by immersing the substrates in a KOH solution (30 wt%) at 40 °C for 20 min. Prior to growth, the substrates were immersed in HF (7%) to yield an oxide-free hydrogen-passivated Si surface, followed by cleaning with deionized water. Finally, the patterned Si (100) substrate was loaded into a metal-organic chemical vapor deposition (MOCVD) reactor (Thomas Swan Scientific Equipment Ltd) for epitaxial growth of GaN, using trimethylgallium (TMG), trimethylaluminum (TMAl), and ammonia (NH_3) as Ga, Al, and N sources, respectively. A thin AlN nucleating layer was selectively grown on the two opposite Si (111) facets at first, then single-compound GaN was synthesized under 1050 °C and 400 mbar in hydrogen for 1800 s using TMG (22 μmol min^{-1}) and NH_3 (67 mmol min^{-1}). AlN ultrathin interlayer was deposited at 1100 °C for 10 s using TMAl (5.3 μmol min^{-1}) and NH_3 (90 mmol min^{-1}). Then AlGaN layer with Al composition of 30% was grown at 1200 °C for 60 s using TMG (12.3 μmol min^{-1}), TMG (4.6 μmol min^{-1}), and NH_3 (110 mmol min^{-1}).

Room-Temperature and Low-Temperature Device Fabrication Process: Room-temperature devices was fabricated by transferring and bonding an individual heterostructure microwire laterally on a polyethylene terephthalate substrate with its *a*-axis in the plane of the substrate. Details about the transferring method and corresponding characterizations of the heterostructured microwire have been described in our previous work.[29–32] Indium tin oxide (ITO) was deposited on both ends of the microwire and served as source and drain electrodes. A thin layer of polydimethylsiloxane (PDMS) was used to package the device for enhancing its robustness as well as protecting it from possible corrosion or contamination in environment.

For low-temperature devices, aluminum foils (76 μm in thickness) covered with a layer of Kapton tape (30 μm in thickness) was used as the substrate (1 × 3 cm^2), which featured with excellent thermal

© 2016 WILEY-VCH Verlag GmbH & Co. KGaA, Weinheim
Adv. Mater. 2016, DOI: 10.1002/adma.201601721

conductivity, an insulating surface, and satisfactory mechanical flexibility. The thermal expansion coefficients of aluminum and Kapton tape were 23.1×10^{-6} and 20×10^{-6} °C^{-1},[26] respectively. Substrate deformations due to the mismatch of thermal expansion coefficients could therefore be neglected. The device was fabricated by transferring and bonding an individual heterostructure microwire laterally on this substrate with its *a*-axis parallel to the long edge. ITO was deposited on both ends of the microwire and served as source and drain electrodes.

External Strain Calculations: External strains along *a*-axis were applied on heterostructure microwires by locking the device in between a 3D mechanical stages (moving resolution ≈10 µm) and a steady rest as shown in Figure 3a. By moving the 3D stages upward or downward, a compressive or tensile strain was applied on the devices. The value of strain applied on the device was calculated following the method reported previously by Yang et al.[33]

Measurements: A function generator (Model no. DS345, Stanford Research Systems, Inc.), a low-noise voltage preamplifier (Model no. SR560, Stanford Research Systems, Inc.), and a low-noise current preamplifier (Model No. SR570, Stanford Research Systems, Inc.) in conjunction with a GPIB controller (GPIB-USB-HS, NI 488.2) were used for electrical measurements. Computer-controlled measurement software was used to collect and record the data.

Supporting Information

Supporting Information is available from the Wiley Online Library or from the author.

Acknowledgements

X.W., R.Y., and C.J. contributed equally to this work. This research was supported by U.S. Department of Energy, Office of Basic Energy Sciences (Award DE-FG02-07ER46394), the National Science Foundation (DMR-1505319), and the "thousands talents" program for pioneer researcher and his innovation team, China. This work was also supported by the National Natural Science Foundation of China (Grant Nos. 51172079 and 11474105) and the Science and Technology Program of Guangdong Province, China (Grant Nos. 2015B090903078 and 2015B010105011).

Received: March 30, 2016
Revised: April 30, 2016
Published online:

[1] W. Guo, M. Zhang, A. Banerjee, P. Bhattacharya, *Nano Lett.* **2010**, *10*, 3355.
[2] F. Qian, S. Gradecak, Y. Li, C. Y. Wen, C. M. Lieber, *Nano Lett.* **2005**, *5*, 2287.
[3] M. H. Huang, S. Mao, H. Feick, H. Q. Yan, Y. Y. Wu, H. Kind, E. Weber, R. Russo, P. D. Yang, *Science* **2001**, *292*, 1897.
[4] F. Qian, Y. Li, S. Gradecak, H. G. Park, Y. J. Dong, Y. Ding, Z. L. Wang, C. M. Lieber, *Nat. Mater.* **2008**, *7*, 701.
[5] Y. Cui, Z. H. Zhong, D. L. Wang, W. U. Wang, C. M. Lieber, *Nano Lett.* **2003**, *3*, 149.
[6] L. J. Lauhon, M. S. Gudiksen, C. L. Wang, C. M. Lieber, *Nature* **2002**, *420*, 57.
[7] Z. L. Wang, J. H. Song, *Science* **2006**, *312*, 242.
[8] C. Y. Chen, G. Zhu, Y. F. Hu, J. W. Yu, J. H. Song, K. Y. Cheng, L. H. Peng, L. J. Chou, Z. L. Wang, *ACS Nano* **2012**, *6*, 5687.
[9] Y. Qin, X. D. Wang, Z. L. Wang, *Nature* **2009**, *457*, 340.
[10] C. K. Jeong, J. Lee, S. Han, J. Ryu, G. T. Hwang, D. Y. Park, J. H. Park, S. S. Lee, M. H. Byun, S. H. Ko, K. J. Lee, *Adv. Mater.* **2015**, *27*, 18.
[11] J. Xiang, W. Lu, Y. J. Hu, Y. Wu, H. Yan, C. M. Lieber, *Nature* **2006**, *441*, 489.
[12] X. Miao, X. L. Li, *IEEE Electron Device Lett.* **2011**, *32*, 1227.
[13] Y. Li, J. Xiang, F. Qian, S. Gradecak, Y. Wu, H. Yan, H. Yan, D. A. Blom, C. M. Lieber, *Nano Lett.* **2006**, *6*, 1468.
[14] O. Ambacher, J. Smart, J. R. Shealy, N. G. Weimann, K. Chu, M. Murphy, W. J. Schaff, L. F. Eastman, R. Dimitrov, L. Wittmer, M. Stutzmann, W. Rieger, J. Hilsenbeck, *J. Appl. Phys.* **2000**, *87*, 334.
[15] S. Vandenbrouck, K. Madjour, D. Theron, Y. J. Dong, Y. Li, C. M. Lieber, C. Gaquiere, *IEEE Electron Device Lett.* **2009**, *30*, 322.
[16] I. P. Smorchkova, L. Chen, T. Mates, L. Shen, S. Heikman, B. Moran, S. Keller, S. P. DenBaars, J. S. Speck, U. K. Mishra, *J. Appl. Phys.* **2002**, *91*, 4780.
[17] Y. F. Zhang, J. Singh, *J. Appl. Phys.* **1999**, *85*, 587.
[18] J. Zhou, Y. D. Gu, P. Fei, W. J. Mai, Y. F. Gao, R. S. Yang, G. Bao, Z. L. Wang, *Nano Lett.* **2008**, *8*, 3035.
[19] R. M. Yu, C. F. Pan, J. Chen, G. Zhu, Z. L. Wang, *Adv. Funct. Mater.* **2013**, *23*, 5868.
[20] R. M. Yu, C. F. Pan, Z. L. Wang, *Energy Environ. Sci.* **2013**, *6*, 494.
[21] C. F. Pan, R. M. Yu, S. M. Niu, G. Zhu, Z. L. Wang, *ACS Nano* **2013**, *7*, 1803.
[22] R. M. Yu, W. Z. Wu, Y. Ding, Z. L. Wang, *ACS Nano* **2013**, *7*, 6403.
[23] O. Ambacher, R. Dimitrov, M. Stutzmann, B. Foutz, M. Murphy, J. Smart, J. R. Shealy, N. G. Weimann, L. F. Eastman, *Inst. Phys. Conf. Ser.* **2000**, 493.
[24] L. Shen, S. Heikman, B. Moran, R. Coffie, N.Q. Zhang, D. Buttari, I. P. Smorchkova, S. Keller, S. P. DenBaars, U. K. Mishra, *IEEE Electron Device Lett.* **2001**, *22*, 10.
[25] R. M. Yu, X. F. Wang, W. Z. Wu, C. F. Pan, Y. Bando, N. Fukata, Y. F. Hu, W. B. Peng, Y. Ding, Z. L. Wang, *Adv. Funct. Mater.* **2015**, *25*, 5277.
[26] Y. F. Hu, B. D. B. Klein, Y. J. Su, S. M. Niu, Y. Liu, Z. L. Wang, *Nano Lett.* **2013**, *13*, 5026.
[27] K. S. Lee, D. H. Yoon, S. B. Bae, M. R. Park, G. H. Kim, *ETRI J.* **2002**, *24*, 270.
[28] M. Kalafi, A. Asgari, *Phys. E* **2003**, *19*, 321.
[29] X. F. Wang, J. H. Tong, X. Chen, B. J. Zhao, Z. W. Ren, D. W. Li, X. J. Zhuo, J. Zhang, H. X. Yi, C. Liu, F. Fang, S. T. Li, *Chem. Commun.* **2014**, *50*, 6.
[30] X. F. Wang, Y. Zhang, X. M. Chen, M. He, C. Liu, Y. A. Yin, X. S. Zou, S. T. Li, *Nanoscale* **2014**, *6*, 20.
[31] R. M. Yu, X. F. Wang, W. B. Peng, W. Z. Wu, Y. Ding, S. T. Li, Z. L. Wang, *ACS Nano* **2015**, *9*, 10.
[32] X. F. Wang, R. M. Yu, W. B. Peng, W. Z. Wu, S. T. Li, Z. L. Wang, *Adv. Mater.* **2015**, *27*, 48.
[33] R. S. Yang, Y. Qin, L. M. Dai, Z. L. Wang, *Nat. Nanotechnol.* **2009**, *4*, 34.

© 2016 WILEY-VCH Verlag GmbH & Co. KGaA, Weinheim